Hydrogeophysical evidences of groundwater exploration potentiality by combined study of electroresistivity and VLF

Daniel Luã S. Miranda[1], Suzan S. de Vasconcelos[1]*, Joelson da C. Batista[1] and Alexsandro G. Cerqueira[1].

[1]Universidade Federal da Bahia.

Abstract

This study presents the result of the geophysical investigation referent the transformation of a swamp area to a drained zone with contraction cracks, related to the seasonality from the surface part of a shallow aquifer. The previous information indicates the presence of a more deep crystalline aquifer, which raises the importance of detecting fractures to determine the potential for your exploration. This research consisted of electroresistivity measurements, using the electrical resistivity imaging interpreted along a line in the NW-SE direction and four lines of Very Low Frequency (VLF) cross measurements. The VLF data were processed by the Fraser and Karous Hjelt filters and analyzed through the components of the polarization ellipse. The interpretation of this data was complemented by the resistivities distribution obtained in the inverted electrical section. The geophysical evidence led to the identification of the basement and two zones of high conductivity (one shallower and the other deeper) that occur in all lines that characterize this underground aquifer.

Introduction

In this research, the study area is Bicudo Farm, located in the municipality of São Gonçalo, Bahia, Brazil (Figure 1). In this region, even though the majority of the population inhabits the urban area, villages and families living on farms far from the city center are registered. Due to this distance and lack of infrastructure, the local population has access to drinking water restricted to semi-artesian wells (deep wells that need a pump). The change of scenery in portions of low topographic regions, of previously drenched to areas drained with contraction cracks during droughts encouraged residents to seek scientific support to obtain information about the localization of a possible underground aquifers in this region.

The hydrogeophysical study developed in this research combined the methods of electroresistivity (ER) and Very Low Frequency (VLF) aiming to characterize the potential of the underground aquifer, localized in the area of Bicudo Farm, for well planning and conscious use of this resource, avoiding possible risks of contamination associated with occupations in adjacent geographical portions. For ER method, we employ the dipole-dipole electrode arrangement (Telford et al., 1976), arrangement

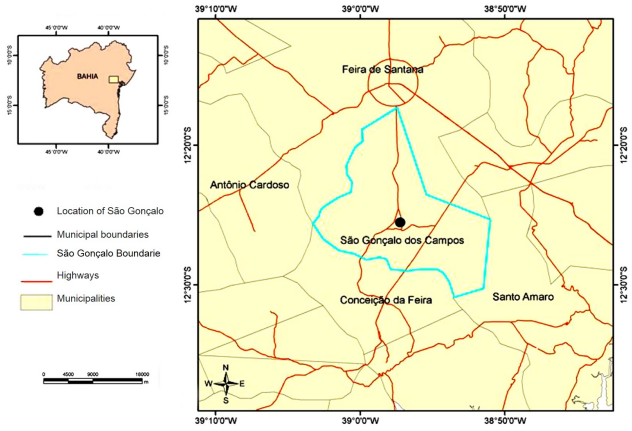

Figure 1: Geographic Location of São Gonçalo dos Campos municipality, modified from Rodrigues (2009).

traditionality employed in the location of the wells and search for accumulations of water and resistive bodies. The VLF electromagnetic method can be employed to detect and locate vertical or sub-vertical fractures and faults at moderate depths, delimiting lateral variations in resistivity (Telford et al., 1976, McNeill and Labson, 1988). In addition, its main advantages are the speed of acquisition and simplicity in handling the equipment. Data were collected, processed, and interpreted over five profiles: a pseudo-section of 2D DC resistivity survey and four measurement lines of VLF. Geological data from CPRM (CPRM, 2018b) supported the geophysical interpretation performed.

Method

Electroresistivity

The electroresistivity method uses an artificial and controlled source of electric current that is injected into the ground through electrodes, so that potentials resultant can be measured through other electrodes coupled to the terrain. The electrical potential V in a conductive homogeneous semi space with semispherical geometry produced by a current injection point, on the surface, is related to the electrical property of resistivity ρ of this medium, through the equation (Telford, 1976):

$$V = \frac{\rho I}{2\pi r}, \tag{1}$$

I is the current intensity of the source, and r is the distance

between de injection and measurement points.

For the realization of the electroresistivity survey, we distribute a set of current and potential electrodes on the ground. The injection of current on the ground by the current electrodes, excited by a source, and the measurements of your variation ΔV by the potential electrodes, together with the geometric factor K, are used to obtain the apparent resistivity ρ_a (Eq. 2):

$$\rho_a = K\frac{\Delta V}{I}. \tag{2}$$

The arrangement of electrodes can provide a one-dimensional (electric vertical drilling) or two-dimensional (electrical tomography) dataset. In this work, the dipole-dipole array was employed to deliver a 2D image of apparent resistivity.

Very Low Frequency method (VLF)

The VLF radio frequency band is a name given to the band between 3 and $30kHz$, but due to the power limitation of the transmitters used, it acts between 5 and $25kHz$ (McNeill and Labson, 1988). The VLF method consists of using a powerful signal radio transmitter for military use, spread worldwide and with global reach. Since 1963, this frequency range has been considered for the prospecting of bodies electrically conductive and tested at known mineral deposit sites (Saydam, 1981). Its principle is the measurement of the magnetic field inclination (dip angle) or the intensity of the horizontal and vertical components of the magnetic fields. It happens because it was found that the magnetic field in the radiofrequency band reached its maximum value on subsurface conductors, and the vertical magnetic field module reached its minimum value in this same position (Zhang, 2015). Due to the wave propagation setting, VLF measurements should be made in a perpendicular direction to the target geological structures.

Filters

The components measured by the VLF system have non-linear and harmonic noises coming from different sources (electrical system and cables, lightning, the VLF-EM transmitter, and other causes.), making it impossible to perform a direct interpretation of this data. The use of filters on this data aims to increase your signal-to-noise ratio and/or remove part of the intrinsic noise from natural and artificial sources (McNeill and Labson, 1988). The most common filters are Fraser (Sundararajan et al., 2007) and Kaorus-Hjelt (Karous and Hjelt, 1983). The Fraser filter is a simple numerical filter that converts crossover points of the polarity into peaks by differentiating successive tilt angle values along with the profile (the first derivative of the data). This filter calculates the horizontal gradient, which produces maximum values for conductors. In other words: it acts on the anomaly so that the parts with maximum inclination will appear as maximum amplitude since it displaces the dip angle by $90°$ (Sundararajan et al., 2007).

The Karous Filter (Karous and Hjelt, 1983) performs linear filtering for the dip angle analysis through the Fraser filter, which is a more generalized version of this filter. The technique is based on filtering the same data set at various depths, thus resulting in a better perception of the variation of current density with depth. Therefore, areas with high current density will qualitatively equate to areas with good conductivity (Sundararajan et al., 2007).

Polarization Ellipse

Components of the electromagnetic field vary in phase and amplitude according to the direction in which it propagates (Marques, 1995). Thus, in the propagation of the VLF signal, the secondary fields generated by currents induced in the non-homogeneous conductive space act with a lag in the primary horizontal field, i. e., thanks to the variation that occurs in the phase and direction over time, the total resulting field is not linearized, and its vector describes a polarization ellipsoid. Thus, the H_z and H_x amplitudes are the vertical and horizontal components of the resulting field, and H_1, H_2 are the major and minor axes of the polarization ellipse and α is the tilt angle (Saydam, 1981), as shown in Figure 2.

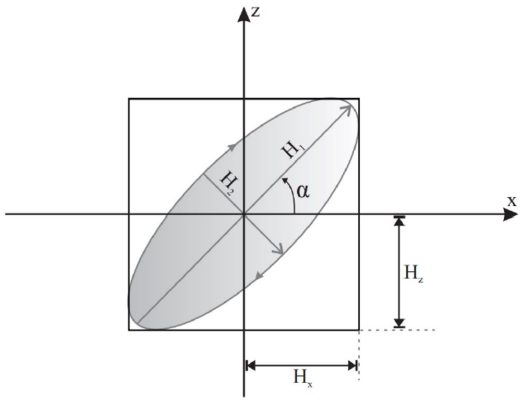

Figure 2: Scheme of the Polarization Ellipse, with the indication of the field components that originate it (H_z and H_x) and the axes of the ellipse (H_1 and H_2), where it is the tilt angle (Conceição, 2010).

The tilt angle (α) is the angle formed between the major axis of the polarization ellipse and one of the coordinate axes, and the ellipsity (ε) is the ratio between the amplitudes of the axes of the ellipse. Both are measured in degrees or as a percentage (Saydam, 1981). Mathematically, they are defined by:

Tilt Angle:

$$\alpha = \pm \arctan\left[\frac{2(H_z/H_x)cos\Delta\phi}{1-(H_z/H_x)^2}\right] \tag{3}$$

Ellipsity:

$$\varepsilon = \frac{H_2}{H_1} = \left[\frac{2(H_zH_x)sin\Delta\phi}{H_2^2}\right] \times 100\%, \tag{4}$$

where the phases of the vertical and horizontal magnetic components equal to, respectively, ϕ_z and ϕ_x, and $\Delta\phi = \phi_z - \phi_x$ is the lag between the vertical and horizontal fields. In equation 3, when $H_x \gg H_z$ (situation of propagation of VLF waves, because the primary field is much larger than the secondary), the ratio $(H_z/H_x)^2$ tends to zero. Therefore, it is possible to rewrite it in a simplified way, such as:

$$\alpha = \pm 1/2 \arctan 2(H_z/H_x). \quad (5)$$

We can rewrite these equations to portray the real and imaginary components, where H_z/H_x is the fraction corresponding to the vertical secondary field. Thus, real and imaginary components are express, respectively, by:

$$Re(H_z) = \frac{H_z}{H_x} \cos\Delta\phi, \quad (6)$$

and

$$Im(H_z) = \frac{H_z}{H_x} \sin\Delta\phi. \quad (7)$$

Consequently, the tilt angle tangent is considered a good approximation for the ratio between the secondary magnetic field real component and the primary magnetic field horizontal component, and the ellipsity is considered a good approximation for the ratio between the vertical secondary magnetic field quadrature component to the horizontal component of the primary magnetic field. These values are called real $(\alpha \times 100\%)$ and imaginary $(\varepsilon \times 100\%)$ anomalies and are expressed in percentage.

Phased Component versus Tilt Angle

The tilt angle is the angle formed between the major polarization ellipse axis and one of the coordinate axes. The ellipsity is the ratio between the amplitudes of the ellipse's axes. In physical terms, they are understood (Bozzo et al., 1994) as the ratio of the real component of the vertical magnetic field ($R_e(H_z)$) with the horizontal primary field (H_p) and the ratio between the imaginary component of the vertical magnetic field ($I_m(H_z)$) with the primary horizontal field H_p (Equation 8 and 9), respectively,

$$\alpha = \frac{Re(H_z)}{H_p}, \quad (8)$$

$$\varepsilon = \frac{Im(H_z)}{H_p}. \quad (9)$$

Results

The study of the aquifer located in the Bicudo Farm area in São Gonçalo dos Campos was carried out using geophysical measurements of VLF and ER. For these measures, we use the T-VLF receiver and the Syscal equipment, both by IRIS Instruments. For VLF measures, we plan four parallel profiles in the NE – SW direction with the distance about of $70m$ in betwen the lines, each one performed with $6m$ spacing stations of measurement. For ER measures, a single profile was made in a perpendicular direction to the VLF profiles and using a dipole-dipole arrangement with spacing between the potential and current electrodes of $20m$ (Figure 3). Figure 3 shows the study region, where the active water well stands out, and a small swamp area that has about $3m^2$. In the database of water wells in the municipality (CPRM, 2018b), we found 35 registered wells, with an average depth was $69m$ and the maximum depth ranged from 14 to $102m$. This information was used for interpretations later.

Figure 3: Scheme of field lines distribution overlapping the map area.

Eletrorresistivity interpretation

In the inverted section (Figure 4), it is possible to observe a low surface resistive highlighted at the beginning of the acquisition line, between 30 and $90m$, indicating a conductive saturated zone. Another low resistivity region is located between stations 120 and 140 at a greater depth of approximately $37m$. This region extends along with the study profile at this depth, and this saturated zone may belong to a fractured aquifer since it is at a depth that is following that reported by the local farmers. A high resistivity zone is well defined at depths greater than $25m$, extending laterally between approximately 45 and $110m$ and presents greater values with depth increases. This resistivity section was inverted with an error of 20.5% and considered adequate for this interpretation.

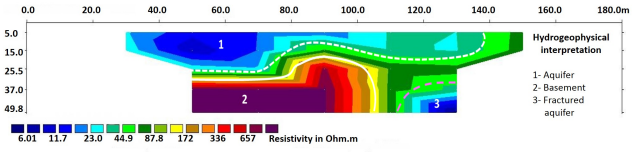

Figure 4: Inverse model resistivity section. The spacing between the potential and current electrodes of the dipole-dipole array was $20m$.

From these interpretations it was possible to define three main features: the superficial portion 1, stands out for its low resistivity and extends superficially for almost the entire section, being approximately $15m$ away from the saturated area (the wetland) and $20m$ away from the water well of the farm. Portion 2 corresponds to the intact crystalline basement evidenced by a sudden transition from low to high resistivity. The depth of the basement is consistent with the data obtained from water wells in the region, in which many reach a crystalline basement between 10 and $15m$ deep after drilling (CPRM, 2018b). Finally, portion 3 indicates the presence of a fractured underground aquifer at depths greater than $37m$.

VLF Interpretation

A qualitative analysis was performed in the VLF data and some spurious values were removed. Subsequently, the data in the frequencies of $18kHz$ and $24kHz$ was compared, to assess which operating frequency obtained the best result. Overall, the $18kHz$ frequency provided more

consistent readings and less noisy.

Tilt Angle and Ellipsity

Figures 5 (lines A, B, C, and D) show the relationship between tilt angle and ellipsity along the lines. Through the analysis of these graphs, it is possible to verify that in a large part of the profile, the magnitude of one of them increases in the proportion that the other decreases. This is a consequence of defining the values in the phase and quadrature about the resulting module. This is quite evident in lines A, B, and C (and a little inline D) of $24kHz$ and in lines A, B, and C of $18kHz$. Crossover points on graphics of lines A of $24kHz$ and C of $18kHz$ are noticeable. These stretches, where there is a crossing of tilt angle and ellipsity data, indicate regions with strong conductivity changes in the medium. Stretches where one curve decreases a lot, while other increases, but without crossover, they can correspond to smoother transitions in conductivity.

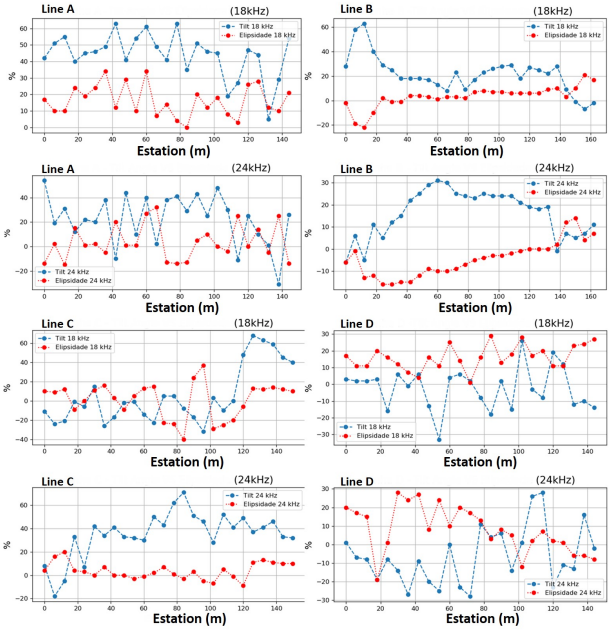

Figure 5: Tilt Angle and Ellipsity (%) by station.

Analysis of Tipper

The Tipper data was calculated through the ratio between the values of the secondary vertical field-induced and the horizontal magnetic field transmitted. This value was used to locate out zones in the acquisition profile in which there is a conducting body since it will represent an increase in the intensity of the secondary field H_z. Thus, the Tipper is a useful parameter to verify conductivity contrasts. In the Figures 6 (Lines A, B, C, and D), there are several maximum points in the Tipper curves. It is important to note that almost all Tipper values are above 100%, meaning that the vertical H_z field is larger than the horizontal H_p field, thus contradicting some initial theoretical expectations. This fact stems from the proximity in which the lines were established concerning the position of the conducting body. Thus, it is clear that the survey with the VLF was all done above the aquifer, implying difficulty in proving conductivity contrast with this analysis alone. The Tipper has plotted along with the treatment of the Karous filter, calculated from the data of $18kHz$ that chosen for this analysis due to your better resolution (Figures 6: Lines A, B, C, and D).

Hjelt-Karous versus Tipper Filtration Analysis

We apply the Karous filter in the VLF profiles for the two frequencies used. However, due to the poor quality of the data, filtering for the $24kHz$ frequency was neglected during this interpretation. Karous filtering was performed using the KHFFILT program (Pirttijärvi, 2004) and is presented in the sections that show the variations of the normal component along with the distance between the stations and the depth, at the bottom of the Figures 6. This allowed us to make a correlation between the Tipper data and those obtained with the Karous filtering along with the VLF profiles.

Through the analysis of the Tipper Profile, in Figure 6 (line A), it is possible to affirm that almost all the measurement points have values above 100, with the presence of 6 peaks, namely: in positions of 10, 40, 60, 85, 108, and $125m$. In Karous filtering, it is possible to observe high-intensity anomalies around the 40 and $60m$ positions, especially. In these two stations, the Tipper assumes, in parallel, the highest values of the line followed by a minimum strong when the secondary vertical magnetic field reaches its lowest values.

In the upper graph of line B (Figure 6), it can be seen that the value of the Tipper remains oscillating along the line, with two maximums in the station at 48 and $136m$. Other points between these two values vary more smoothly, despite smaller peaks at the 96 and $108m$ positions. The value of the real component (which represents the conductivity) in this line is not highly variable as in line A. It is possible to point out some minimums in the ranges of 150, 60, and $40m$, but not as severe as the compared to line A graphs (Figure 6).

The values observed from the Tipper, in line C (Figure 6), are approximately constant at the beginning of this profile, with values between 150 and $200m$. From $40m$, there is a noticeable oscillation in the subsequent stations, with measures reaching more than 700% of value in the 48 and $60m$ stations. This oscillation continues until the end of the line. In Karous filtering, although the first $40m$ of acquisition has an approximately constant value, there are two portions with very high conductivity. In the smaller zone between 50 and $65m$, and the largest, ranging from 100 to $130m$ (going from the surface to the maximum depth of the profile). Between these two regions, there are low values in the shallow parts of the profile going up to $10m$ deep (distance between 30 to $40m$, 55 to $60m$ e 75 to $90m$) and deeper between 15 and $25m$ (distance in the range between 70 at $80m$ and the 90 and $100m$ of the line).

In the graphs shown, it is possible to notice changes in the intensities of the current densities in the final stations, but that it shifts a little depending on the line. The mentioned region (Figure 6) corresponds to 80 to $100m$ on line B, 90 to $130m$ on line C, and in line D to positions between 90

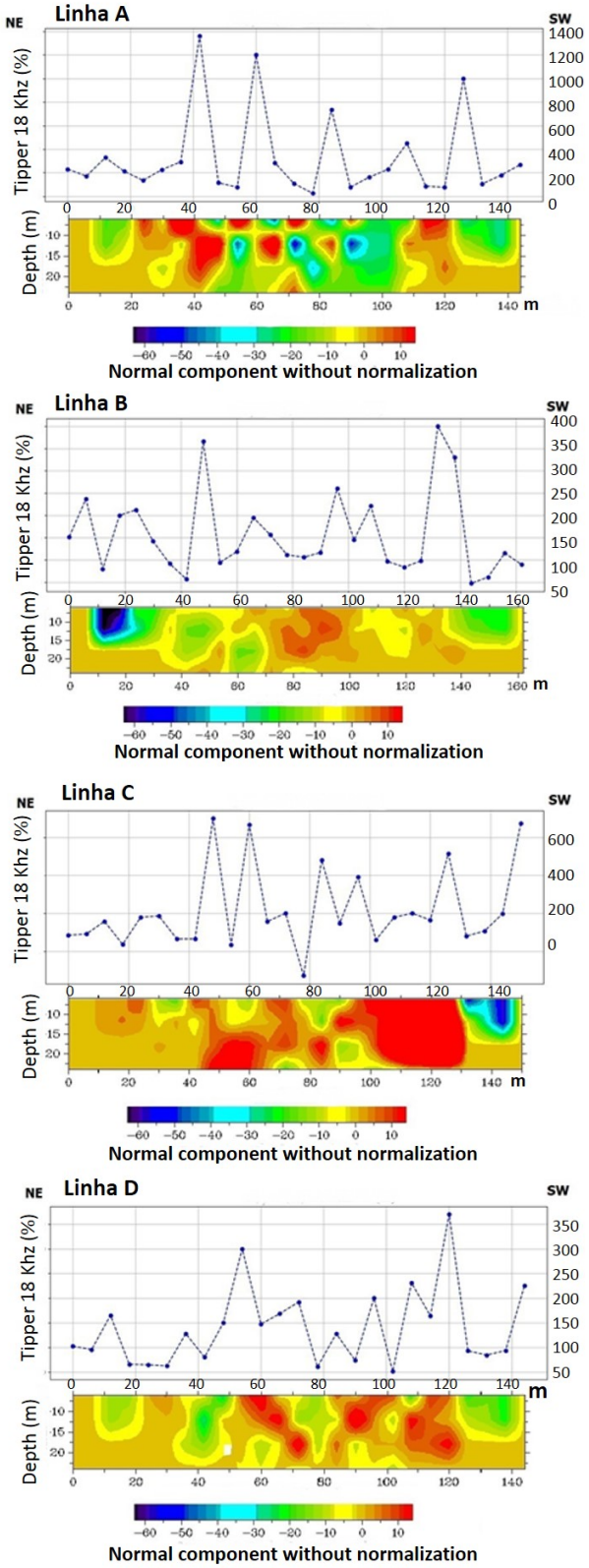

Figure 6: Tipper plot per station (above) and Karous filtration versus station (below) for the frequency of $18kHz$.

to $100m$ and 110 to $120m$. In the SE direction, this region crosses the VLF lines, which could be the result of the saturated zone since it is a very close and/or coincident region of that conducting region considered in Figure 4 in your SE direction.

Due to the extensive anomaly, as well as its large value in line C between approximately 100 and $130m$, it is also possible that these high values in this part of the profile are an indication of the extension of the area identified as 3 in the resistivity profile (Figure 6). The fact of the water well is close in this area, between lines B and C, corroborates with this hypothesis since a region of conductivity is present in lines B, C, and D between 100 and $130m$. It is also noted that some anomalies imply low conductivity in all lines, in different intensities. The most evident example has two anomalies: between 0 and $30m$ as well as 120 and $140m$ approximately, which are well highlighted. It is possible to notice another anomaly approximately between 30 and $50m$ in lines A, B, and C, which may be the limits and more resistive zones of the aquifer.

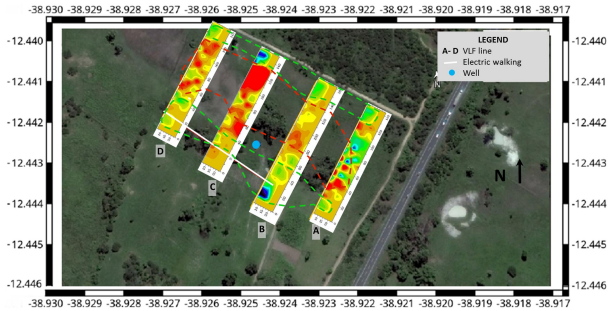

Figure 7: Sections of Karous filtration versus station for the frequency of $18kHz$ overlapping the map area. Dashed line circumvent the trend that indicates the influence of superficial aquifer (green) and basement (red).

Bearing in mind that the responses of Karous filtering are vertical slices, we organized a presentation of the four lines of VLF data filtered by Karous to assess the continuity of features, creating a pseudo-3D interpretation Figure 7. This broader view of the relationship between survey lines in the interpretation of the normal components of the VLF (Figure 7) indicates the areas of the biggest influence of the superficial aquifer in low values of the component which is reaffirmed by the low values of resistivity in electrical section (Figure 4). On other hand, the high component values would indicate the most superficial crystalline rock with fractured areas being indicated by sudden decreases. At the beginning of the VLF line B there is a maximum in the conductivity, due to the superposition of the influence of fractures in the crystalline aquifer with the saturated zone, which was also marked at the end of the resistivity profile.

Conclusions

With the VLF and electroresistivity data study, it was possible to observe a very conductive region, evidence of a saturated zone. This statement was supported by the low resistivity zone, presented in the electroresistivity profile, and high current density values extracted from the data VLF. The anomalies observed in the sections presented with Karous filtering and by the maps at different depths demonstrate their limits in the respective depths and, consequently, of the structures they represent.

The electroresistance and VLF data complemented each other in the results of this work. With the first, it was possible to detect the location of two areas of high conductivity as well as some features of high resistivity present in the four data lines acquired. With the VLF data, it was possible to verify anomalies (which imply high conductivity) extending over the study area. Particularly, the anomaly that is well highlighted between 100 and $130m$ inline C (Figure 6) extends along lines B and D. In this way, it is possible to conclude that this saturated zone covers an area well greater than those detected by the inversion of electroresistivity and the anomalies of the filters.

It is important to note that even though only a single line of electroresistivity acquisition was performed, it only intercepted a small fraction of lines B, C, and D, but this allowed the characterization of this region. Thus, it is concluded that region 1 of Figure 4 is only a saturated surface zone. Area 3, in Figure 4, can indicate the presence of a saturated zone within the crystalline basement since it only appears from $40m$ deep, indicating that it is a region of the crystalline basement and this area is interpreted as a fractured aquifer. Therefore it is possible to say that the results obtained by the work were satisfactory.

Acknowledgement

We would like to thank the Sodré family for permission to do geophysical fieldwork on their property and to Research Center in Geophysics and Geology (CPGG/UFBA) for the technical support to this research.

References

Bozzo, E.; Merlanti, F. e Lombardo, S. 1994. VLF prospecting- Observations about Field experiments, Annali di geofisica, Istituto Nazionale di Geofisica e Vulcanologia, Napoli, Itália, 37(5).

Conceição, T. 2010. Modelagem VLF-EM aplicada à interpretação da relação de contato entre a Bacia De Camamu e seu embasamento adjacente na região de Valença, Bahia, Trabalho de graduação, Universidade Federal da Bahia, Salvador, Brasil.

CPRM. 2018a. Dados, Informações e Produtos do Serviço Geológico do Brasil, Disponível em: <http://geosgb.cprm.gov.br>. Acesso em: 15 de Abril de 2018.

CPRM. 2018b. Sistema de Informações de Águas Subterrâneas. Disponível em: <http://siagasweb.cprm.gov.br/>. Acesso em: 16 de Abril de 2018.

IBGE- Instituto Brasileiro de Geografia e Estatística: Panorama do Município de São Gonçalo dos Campos- BA, 2018. Disponível em: <https://cidades.ibge.gov.br/brasil/ba/sao-goncalo-dos-campos/panorama>. Acesso em: 15 de Abril de 2018.

Karous, M. e Hjelt, S. 1983. Linear Filtering of VLF Dip-Angle Measurements: Geophysical prospecting, Wiley Online Library, Netherlands, 31(5):782-794.

Lima, O. 2014. Propriedades Físicas das Rochas- Bases da Geofísica Aplicada: Sociedade Brasileira de Geofísica, Rio de Janeiro.

Marques, R. M. 1995. Utilização do VLF (Very Low Frequency) na Prospecção de Água Subterrânea em zonas de Rochas Cristalinas, Dissert. de Mestrado, Universidade de São Paulo, São Paulo, Brasil.

McNeill, J. D. e Labson, V. 1988. Electromagnetic theory for geophysical applications, In: M. N. Nabighian, ed., Electromagnetic Methods in Applied Geophysics, vol. 2, Application, Parts A and B, pp. 521-637, Society of Exploration Geophysicists, Netherlands.

Pirttijárvi, M. 2004. KHFfilt Program, A geophysical software for Karous-Hjelt and Fraser Filtering on Geophysical VLF (Very-Low-Frequency) data: Geopysics Division, Department of Geosciences, University of Oulu, Finland.

Rodrigues, D. 2009. Mapeamento preliminar da cobertura e uso do solo no município de são gonçalo dos campos: Anais do XIII Simpósio Brasileiro de Geografia Física Aplicada, Viçosa, MG.

Saydam, A.S. 1981. Very Low-Frequency Electromagnetic Interpretation using Tilt Angle and Ellipticity Measurements, Geophysics: Society of Exploration Geophysicists, Tulsa, Oklahoma, 6(11):1594-1605.

Sundararajan, N.; Nandakumar, G.; Chary, M. N.; Ramam, K. e Srinivas, Y. 2007. VES and VLF-An application to Groundwater Exploration, Khammam, India: The Leading Edge, Society of Exploration Geophysicists, Netherlands, 26(6):708-716.

Telford, W. M.; Geldart, L. P.; Sheriff, R. E. e Keys, D. A. 1976. Applied Geophysics: Cambridge University Press, Cambridge, United Kingdom, Vol. 1.

Zhang, Z. (2015). The Geophysical Very Low Frequency Electromagnetic- Efects Of Topography And Surface Water Investigated With Simulations And Field Measurements: Dissert. de mestrado, University of Saskatchewan, Saskatoon, Saskatchewan, Canada.